Biomedical Optics EXPRESS

Extended coherence length megahertz FDML and its application for anterior segment imaging

Wolfgang Wieser,[1] Thomas Klein,[1] Desmond C. Adler,[2] Francois Trépanier,[3] Christoph M. Eigenwillig,[1] Sebastian Karpf,[1] Joseph M. Schmitt,[2] and Robert Huber[1,*]

[1]*Lehrstuhl für BioMolekulare Optik, Fakultät für Physik, Ludwig-Maximilians-Universität München, Oettingenstr. 67, 80538 Munich, Germany*

[2]*LightLab Imaging, a St. Jude Medical subsidiary, Westford, MA, USA*

[3]*TeraXion Inc., Quebec City, Canada*

**Robert.Huber@Physik.Uni-Muenchen.DE*

Abstract: We present a 1300 nm Fourier domain mode locked (FDML) laser for optical coherence tomography (OCT) that combines both, a high 1.6 MHz wavelength sweep rate and an ultra-long instantaneous coherence length for rapid volumetric deep field imaging. By reducing the dispersion in the fiber delay line of the FDML laser, the instantaneous coherence length and hence the available imaging range is approximately quadrupled compared to previously published MHz-FDML setups, the imaging speed is increased by a factor of 16 compared to previous extended coherence length results. We present a detailed characterization of the FDML laser performance. We demonstrate for the first time MHz-OCT imaging of the anterior segment of the human eye. The OCT system provides enough imaging depth to cover the whole range from the top surface of the cornea down to the crystalline lens.

© 2012 Optical Society of America

OCIS codes: (170.4500) Optical coherence tomography; (110.4500) Optical coherence tomography; (140.3600) Lasers, tunable.

References and links

1. D. Huang, E. A. Swanson, C. P. Lin, J. S. Schuman, W. G. Stinson, W. Chang, M. R. Hee, T. Flotte, K. Gregory, C. A. Puliafito, and J. G. Fujimoto, "Optical coherence tomography," Science **254**(5035), 1178–1181 (1991).
2. A. F. Fercher, C. K. Hitzenberger, G. Kamp, and S. Y. Elzaiat, "Measurement of intraocular distances by backscattering spectral interferometry," Opt. Commun. **117**(1-2), 43–48 (1995).
3. G. Häusler and M. W. Lindner, "'Coherence radar' and 'spectral radar'—new tools for dermatological diagnosis," J. Biomed. Opt. **3**(1), 21–31 (1998).
4. M. A. Choma, M. V. Sarunic, C. H. Yang, and J. A. Izatt, "Sensitivity advantage of swept source and Fourier domain optical coherence tomography," Opt. Express **11**(18), 2183–2189 (2003).
5. J. F. de Boer, B. Cense, B. H. Park, M. C. Pierce, G. J. Tearney, and B. E. Bouma, "Improved signal-to-noise ratio in spectral-domain compared with time-domain optical coherence tomography," Opt. Lett. **28**(21), 2067–2069 (2003).
6. R. Leitgeb, C. K. Hitzenberger, and A. F. Fercher, "Performance of Fourier domain vs. time domain optical coherence tomography," Opt. Express **11**(8), 889–894 (2003).
7. S. H. Yun, G. J. Tearney, J. F. de Boer, N. Iftimia, and B. E. Bouma, "High-speed optical frequency-domain imaging," Opt. Express **11**(22), 2953–2963 (2003).
8. R. Huber, M. Wojtkowski, and J. G. Fujimoto, "Fourier domain mode locking (FDML): a new laser operating regime and applications for optical coherence tomography," Opt. Express **14**(8), 3225–3237 (2006).
9. R. Huber, D. C. Adler, and J. G. Fujimoto, "Buffered Fourier domain mode locking: unidirectional swept laser sources for optical coherence tomography imaging at 370,000 lines/s," Opt. Lett. **31**(20), 2975–2977 (2006).
10. S. H. Yun, G. J. Tearney, B. J. Vakoc, M. Shishkov, W. Y. Oh, A. E. Desjardins, M. J. Suter, R. C. Chan, J. A. Evans, I. K. Jang, N. S. Nishioka, J. F. de Boer, and B. E. Bouma, "Comprehensive volumetric optical microscopy *in vivo*," Nat. Med. **12**(12), 1429–1433 (2006).
11. D. C. Adler, Y. Chen, R. Huber, J. Schmitt, J. Connolly, and J. G. Fujimoto, "Three-dimensional endomicroscopy using optical coherence tomography," Nat. Photonics **1**(12), 709–716 (2007).
12. R. Huber, D. C. Adler, V. J. Srinivasan, and J. G. Fujimoto, "Fourier domain mode locking at 1050 nm for ultra-high-speed optical coherence tomography of the human retina at 236,000 axial scans per second," Opt. Lett. **32**(14), 2049–2051 (2007).

#172420 - $15.00 USD Received 13 Jul 2012; rev. 14 Sep 2012; accepted 15 Sep 2012; published 24 Sep 2012
(C) 2012 OSA

13. B. Potsaid, I. Gorczynska, V. J. Srinivasan, Y. L. Chen, J. Jiang, A. Cable, and J. G. Fujimoto, "Ultrahigh speed spectral / Fourier domain OCT ophthalmic imaging at 70,000 to 312,500 axial scans per second," Opt. Express **16**(19), 15149–15169 (2008).
14. B. Potsaid, B. Baumann, D. Huang, S. Barry, A. E. Cable, J. S. Schuman, J. S. Duker, and J. G. Fujimoto, "Ultrahigh speed 1050nm swept source/Fourier domain OCT retinal and anterior segment imaging at 100,000 to 400,000 axial scans per second," Opt. Express **18**(19), 20029–20048 (2010).
15. V. Jayaraman, J. Jiang, H. Li, P. Heim, G. Cole, B. Potsaid, J. G. Fujimoto, and A. Cable, "OCT imaging up to 760kHz axial scan rate using single-mode 1310nm MEMs-tunable VCSELs with >100nm tuning range," in *CLEO:2011—Laser Applications to Photonic Applications*, OSA Technical Digest (CD) (Optical Society of America, 2011), paper PDPB2.
16. V. Jayaraman, J. Jiang, B. Potsaid, G. Cole, J. Fujimoto, and A. Cable, "Design and performance of broadly tunable, narrow line-width, high repetition rate 1310nm VCSELs for swept source optical coherence tomography," Proc. SPIE **8276**, 82760D, 82760D-11 (2012).
17. Y. Yasuno, V. D. Madjarova, S. Makita, M. Akiba, A. Morosawa, C. Chong, T. Sakai, K. P. Chan, M. Itoh, and T. Yatagai, "Three-dimensional and high-speed swept-source optical coherence tomography for *in vivo* investigation of human anterior eye segments," Opt. Express **13**(26), 10652–10664 (2005).
18. R. Huber, M. Wojtkowski, K. Taira, J. G. Fujimoto, and K. Hsu, "Amplified, frequency swept lasers for frequency domain reflectometry and OCT imaging: design and scaling principles," Opt. Express **13**(9), 3513–3528 (2005).
19. C. M. Eigenwillig, B. R. Biedermann, W. Wieser, and R. Huber, "Wavelength swept amplified spontaneous emission source," Opt. Express **17**(21), 18794–18807 (2009).
20. C. M. Eigenwillig, T. Klein, W. Wieser, B. R. Biedermann, and R. Huber, "Wavelength swept amplified spontaneous emission source for high speed retinal optical coherence tomography at 1060 nm," J Biophotonics **4**(7-8), 552–558 (2011).
21. B. R. Biedermann, W. Wieser, C. M. Eigenwillig, and R. Huber, "Recent developments in Fourier domain mode locked lasers for optical coherence tomography: imaging at 1310 nm vs. 1550 nm wavelength," J Biophotonics **2**(6-7), 357–363 (2009).
22. B. Golubovic, B. E. Bouma, G. J. Tearney, and J. G. Fujimoto, "Optical frequency-domain reflectometry using rapid wavelength tuning of a Cr^{4+}:forsterite laser," Opt. Lett. **22**(22), 1704–1706 (1997).
23. C. M. Eigenwillig, W. Wieser, B. R. Biedermann, and R. Huber, "Subharmonic Fourier domain mode locking," Opt. Lett. **34**(6), 725–727 (2009).
24. W. Wieser, B. R. Biedermann, T. Klein, C. M. Eigenwillig, and R. Huber, "Multi-megahertz OCT: high quality 3D imaging at 20 million A-scans and 4.5 GVoxels per second," Opt. Express **18**(14), 14685–14704 (2010).
25. T. Klein, W. Wieser, C. M. Eigenwillig, B. R. Biedermann, and R. Huber, "Megahertz OCT for ultrawide-field retinal imaging with a 1050 nm Fourier domain mode-locked laser," Opt. Express **19**(4), 3044–3062 (2011).
26. J. Zhang, G. J. Liu, and Z. P. Chen, "Ultra broad band Fourier domain mode locked swept source based on dual SOAs and WDM couplers," Proc. SPIE **7554**, 75541I, 75541I-5 (2010).
27. Y. X. Mao, C. Flueraru, S. D. Chang, and S. Sherif, "High-power 1300 nm FDML swept laser using polygon-based narrowband optical scanning filter," Proc. SPIE **7168**, 716822, 716822-8 (2009).
28. S. Marschall, T. Klein, W. Wieser, B. R. Biedermann, K. Hsu, K. P. Hansen, B. Sumpf, K.-H. Hasler, G. Erbert, O. B. Jensen, C. Pedersen, R. Huber, and P. E. Andersen, "Fourier domain mode-locked swept source at 1050 nm based on a tapered amplifier," Opt. Express **18**(15), 15820–15831 (2010).
29. D. C. Adler, W. Wieser, F. Trepanier, J. M. Schmitt, and R. A. Huber, "Extended coherence length Fourier domain mode locked lasers at 1310 nm," Opt. Express **19**(21), 20930–20939 (2011).
30. E. Osiac, A. Săftoiu, D. I. Gheonea, I. Mandrila, and R. Angelescu, "Optical coherence tomography and Doppler optical coherence tomography in the gastrointestinal tract," World J. Gastroenterol. **17**(1), 15–20 (2011).
31. J. A. Izatt, M. R. Hee, E. A. Swanson, C. P. Lin, D. Huang, J. S. Schuman, C. A. Puliafito, and J. G. Fujimoto, "Micrometer-scale resolution imaging of the anterior eye *in vivo* with optical coherence tomography," Arch. Ophthalmol. **112**(12), 1584–1589 (1994).
32. M. Hagen-Eggert, P. Koch, and G. Huttmann, "Analysis of the signal fall-off in spectral domain optical coherence tomography systems," Proc. SPIE **8213**, 82131K, 82131K-7 (2012).
33. B. Potsaid, V. Jayaraman, J. G. Fujimoto, J. Jiang, P. J. S. Heim, and A. E. Cable, "MEMS tunable VCSEL light source for ultrahigh speed 60kHz-1MHz axial scan rate and long range centimeter class OCT imaging," Proc. SPIE **8213**, 82130M (2012).
34. B. Považay, B. Hofer, C. Torti, B. Hermann, A. R. Tumlinson, M. Esmaeelpour, C. A. Egan, A. C. Bird, and W. Drexler, "Impact of enhanced resolution, speed and penetration on three-dimensional retinal optical coherence tomography," Opt. Express **17**(5), 4134–4150 (2009).
35. L. An, G. Guan, and R. K. Wang, "High-speed 1310 nm-band spectral domain optical coherence tomography at 184,000 lines per second," J. Biomed. Opt. **16**(6), 060506 (2011).
36. L. An, P. Li, T. T. Shen, and R. Wang, "High speed spectral domain optical coherence tomography for retinal imaging at 500,000 A-lines per second," Biomed. Opt. Express **2**(10), 2770–2783 (2011).
37. B. Baumann, B. Potsaid, M. F. Kraus, J. J. Liu, D. Huang, J. Hornegger, A. E. Cable, J. S. Duker, and J. G. Fujimoto, "Total retinal blood flow measurement with ultrahigh speed swept source/Fourier domain OCT," Biomed. Opt. Express **2**(6), 1539–1552 (2011).

#172420 - $15.00 USD Received 13 Jul 2012; rev. 14 Sep 2012; accepted 15 Sep 2012; published 24 Sep 2012
(C) 2012 OSA

38. W.-Y. Oh, B. J. Vakoc, M. Shishkov, G. J. Tearney, and B. E. Bouma, ">400 kHz repetition rate wavelength-swept laser and application to high-speed optical frequency domain imaging," Opt. Lett. **35**(17), 2919–2921 (2010).
39. T. Bonin, G. Franke, M. Hagen-Eggert, P. Koch, and G. Hüttmann, "*In vivo* Fourier-domain full-field OCT of the human retina with 1.5 million A-lines/s," Opt. Lett. **35**(20), 3432–3434 (2010).
40. D. Choi, H. Hiro-Oka, H. Furukawa, R. Yoshimura, M. Nakanishi, K. Shimizu, and K. Ohbayashi, "Fourier domain optical coherence tomography using optical demultiplexers imaging at 60,000,000 lines/s," Opt. Lett. **33**(12), 1318–1320 (2008).
41. R. Wang, J. X. Yun, R. Goodwin, R. Markwald, T. K. Borg, R. B. Runyan, and B. Gao, "4D imaging of embryonic chick hearts by streak-mode Fourier domain optical coherence tomography," Proc. SPIE **8207**, 82073V, 82073V-6 (2012).
42. R. Wang, J. X. Yun, X. Yuan, R. Goodwin, R. R. Markwald, and B. Z. Gao, "Megahertz streak-mode Fourier domain optical coherence tomography," J. Biomed. Opt. **16**(6), 066016 (2011).
43. B. R. Biedermann, W. Wieser, C. M. Eigenwillig, T. Klein, and R. Huber, "Dispersion, coherence and noise of Fourier domain mode locked lasers," Opt. Express **17**(12), 9947–9961 (2009).
44. W. Wieser, B. R. Biedermann, T. Klein, C. M. Eigenwillig, and R. Huber, "Ultra-rapid dispersion measurement in optical fibers," Opt. Express **17**(25), 22871–22878 (2009).
45. B. R. Biedermann, W. Wieser, C. M. Eigenwillig, G. Palte, D. C. Adler, V. J. Srinivasan, J. G. Fujimoto, and R. Huber, "Real time en face Fourier-domain optical coherence tomography with direct hardware frequency demodulation," Opt. Lett. **33**(21), 2556–2558 (2008).
46. C. M. Eigenwillig, B. R. Biedermann, G. Palte, and R. Huber, "K-space linear Fourier domain mode locked laser and applications for optical coherence tomography," Opt. Express **16**(12), 8916–8937 (2008).
47. B. D. Goldberg, B. J. Vakoc, W. Y. Oh, M. J. Suter, S. Waxman, M. I. Freilich, B. E. Bouma, and G. J. Tearney, "Performance of reduced bit-depth acquisition for optical frequency domain imaging," Opt. Express **17**(19), 16957–16968 (2009).
48. T. Klein, W. Wieser, R. Andre, T. Pfeiffer, C. M. Eigenwillig, and R. Huber, "Multi-MHz FDML OCT: snapshot retinal imaging at 6.7 million axial-scans per second," Proc. SPIE **8213**, 82131E, 82131E-6 (2012).
49. S. Martinez-Conde, S. L. Macknik, X. G. Troncoso, and D. H. Hubel, "Microsaccades: a neurophysiological analysis," Trends Neurosci. **32**(9), 463–475 (2009).
50. M. Gora, K. Karnowski, M. Szkulmowski, B. J. Kaluzny, R. Huber, A. Kowalczyk, and M. Wojtkowski, "Ultra high-speed swept source OCT imaging of the anterior segment of human eye at 200 kHz with adjustable imaging range," Opt. Express **17**(17), 14880–14894 (2009).

1. Introduction

Optical coherence tomography (OCT) is a depth-resolved imaging modality which provides three-dimensional (3D) information of the scattering properties of biological samples at micrometer-scale resolution with millimeter-scale axial imaging ranges [1]. Initially, the slow data acquisition speed of early time domain (TD) OCT systems in the range of ~1kHz usually limited OCT imaging to single B-frame acquisition protocols. This changed with the introduction of frequency domain (or Fourier domain; FD) detection techniques for optical coherence tomography with higher sensitivity [2–7] and a much higher imaging speed. Depth scan rates of ~50-200 kHz are now common for both spectrometer-based (SD-OCT) and swept-source OCT (SS-OCT, also called optical frequency domain imaging, OFDI) [8–17]. Unlike TD-OCT, all FD-OCT systems exhibit a more or less pronounced sensitivity decay over imaging depth . This effect is commonly called "roll-off."

SS-OCT uses spectrally narrowband rapidly wavelength swept light sources, most often these are lasers [7,8,17,18]. However, for very high speed imaging, incoherent, dynamically filtered amplified spontaneous emission sources have been used, too [19,20]. For highly scattering tissue, center wavelengths around 1300nm are most common, but 1550nm can also provide good image quality [21]. The tunable light source is the most critical component of a high-speed SS-OCT system since it determines the overall imaging system performance [7,18,22,23]. The sweep rate, tuning range, and instantaneous coherence length of the light source determine the imaging speed, axial resolution, and imaging range of the SS-OCT system, respectively. The output power and noise of the light source also strongly influence the sensitivity of the SS-OCT system. Fourier domain mode locked (FMDL) lasers [8] are an interesting choice for SS-OCT systems due to their ability to provide extremely high sweep rates of up to several MHz [24,25], broad tuning ranges of up to 200 nm [11,26], and output powers of up to 40 mW [24,25,27,28]. However, previously reported FDML lasers with MHz

#172420 - $15.00 USD Received 13 Jul 2012; rev. 14 Sep 2012; accepted 15 Sep 2012; published 24 Sep 2012
(C) 2012 OSA

tuning speeds suffered a rather steep roll-off performance with a −6dB imaging depth of ≤2 mm. While this is sufficient for highly scattering tissue such as skin, where the penetration depth is limited by loss of backscattered light rather than sensitivity roll-off [21], many applications require better roll-off performance. E.g., for intravascular imaging [29] and gastrointestinal imaging [30], the penetration into the tissue is usually ≤2 mm [21], but the distance to the sample can vary by several millimeters. Another application is *in vivo* OCT imaging of the anterior segment of the human eye, a low-scattering sample with an optical depth of ~6 mm [31]. This will be demonstrated in this paper at MHz A-scan rates.

SD-OCT systems usually have poorer roll-off performance due to limitations in the optical layout of the spectrometer [32]. Time-domain systems, on the other hand, do not suffer any roll-off at all but are limited in speed and offer less sensitivity than Fourier domain setups [4–6]. An *ideal* SS-OCT system would feature an "infinite" roll-off, like a TD-OCT. This would require a light source without coherence decay. Recently presented VCSEL-based sources come very close to this and offer excellent roll-off performance at speeds of typically 100 – 500 kHz. Although up to 1.0 MHz has been reported [15,16,33] for shallow samples, imaging of samples with depth ranges of 6mm or more, like the anterior segment, was limited to 100kHz.

Often, for SS-OCT as well as for SD-OCT, increasing the imaging speed degrades the roll-off performance. For many applications, line rates in excess of several 100 kHz, ideally even more than 1 MHz, are desirable to cover large sample areas quickly and to avoid motion artifacts [14–16,24,25,34–39]. When aiming at high speed, SS-OCT combines several advantages over SD-OCT such as balanced detection, higher available power and better roll-off characteristics. With FDML-based SS-OCT, imaging speeds of up to 4 x 5.2 MHz have been demonstrated [24].

While good roll-off [14–16,29] and high speed [24,25,36,38–42] have been demonstrated *separately*, here for the first time we show >1 MHz 3D OCT imaging speed *and* good roll-off at the same time: our new FDML-based SS-OCT combines a 16x speed improvement over the previously published dispersion compensated FDML laser [29] with a ~4-fold improved roll-off compared to our previous MHz-OCT setups [24]. It provides a line rate of 1.6 MHz at 100 nm sweep range and 10 µm resolution in tissue and features a roll-off figure of ~1.2 mm/dB at a detection bandwidth limited −6 dB imaging depth of 4.9 mm. The key to extending the roll-off performance was to increase the FDML laser coherence by reducing the dispersion in the FDML cavity [29,43,44].

2. Experimental setup

2.1. Dispersion compensated FDML laser

An FDML laser is a high speed wavelength swept light source containing a tunable optical filter in a fiber-based laser cavity. For FDML operation, the cavity round trip time of the light is synchronized to the tuning rate of the wavelength filter. While this provides the advantage of no fundamental limit to the laser tuning rate, the relatively long delay line (usually ~km) introduces substantial chromatic dispersion. Consequently, the FDML criterion, which demands synchronization of filter sweep period and the optical round trip time, cannot be fulfilled for all wavelengths simultaneously. Therefore, the effect of dispersion limits the instantaneous coherence length of an FDML laser.

Dispersion in the 1550 nm telecom wavelength range can be compensated using special dispersion compensation fiber. It has been demonstrated that this improves the instantaneous coherence length of an FDML laser operating at 50 kHz [43]. In contrast to operation around 1550nm, the 1310 nm window is already centered near the zero dispersion wavelength of standard telecom fiber such as SMF-28, so the dispersion is already greatly reduced to typically 0.09 ps/nm^2/km. For a tuning range of 100 nm and a 1 km fiber length, this still results in 220 ps time of flight mismatch. There is no off-the-shelf compensation fiber

#172420 - $15.00 USD Received 13 Jul 2012; rev. 14 Sep 2012; accepted 15 Sep 2012; published 24 Sep 2012
(C) 2012 OSA

available for the 1310 nm window and dispersion compensation is complicated by the fact that both normal and anomalous dispersion occurs. A solution is the use of a specially designed dispersion compensation module (DCM) which has recently been demonstrated to increase FDML coherence length at 80 kHz [29]. Here, we demonstrate the first dispersion compensated laser around 1310 nm which is suitable for OCT imaging rates in the MHz range.

Figure 1 shows a schematic of the FDML laser resonator and the following 4x buffer stage [9]. The FDML laser has a 2.5 km long cavity built in sigma ring configuration and includes a DCM to reduce the total roundtrip time difference over a 100 nm range down to ~5 ps. The DCM consists of a 4-port circulator with two reflective fiber Bragg gratings (FBG) made by Teraxion Inc. These gratings were designed specifically to compensate both the normal as well as the anomalous dispersion introduced by a double-pass through 1.25 km of Corning SFM28e + standard single-mode fiber used in the delay spool. Due to the fiber length, the fundamental FDML round-trip frequency is 80 kHz. For higher speed, the setup employs a Fabry-Pérot tunable filter (FP-TF) driven at 400 kHz [24], so the FDML cavity is operated in the 5th harmonic. The circulators in the cavity were arranged such that they can replace the isolators usually placed before and after the SOA. The high speed laser diode controller in the laser cavity (WL-LDC10D, wieserlabs.com) modulates the SOA current such that the laser is only switched on for 25% of the time [45]. The phase of this modulation is adjusted such that it coincides with the most linear part of the sinusoidal wavelength sweep [46]. The resulting 625 ns long wavelength sweep with 25% duty cycle is delayed and time-interleaved with copies of the original sweep in the following 4x buffer stage [9]. This results in a 100% duty cycle at a sweep rate of 1.6 MHz. A second booster SOA (Covega Inc.) after the buffer stage provides increased output power for OCT imaging.

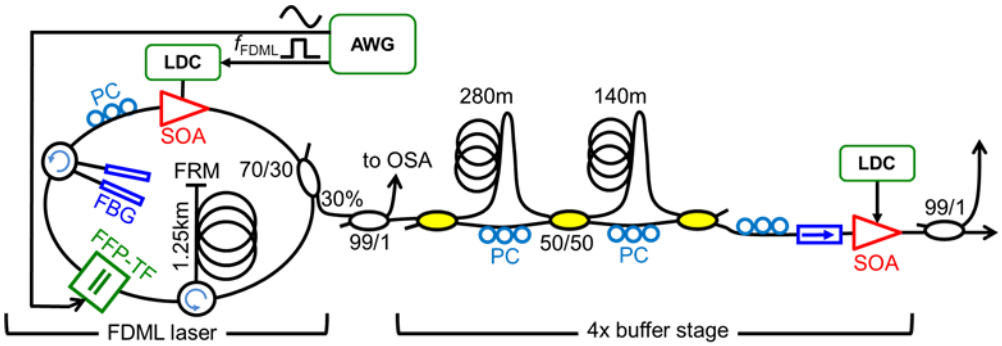


Fig. 1. Schematic of the high speed FDML laser with dispersion compensated cavity followed by a 4x buffer stage. SOA: semiconductor optical amplifier, FBG: fiber Bragg grating, PC: polarization controller, LDC: laser diode controller, FRM: Faraday rotation mirror, FFP-TF: Fabry-Pérot tunable filter, ISO: isolator, AWG: Arbitrary waveform generator, OSA: optical spectrum analyzer.

2.2. OCT interferometer and data acquisition

The OCT interferometer is built in a Mach-Zehnder configuration employing a circulator in each arm as shown in Fig. 2. The power after the booster is attenuated by means of a not fully mated fiber joint to reduce the sample power as to comply with laser safety standards. The reference arm power is adjusted to ~100 µW by slight misalignment of the free space reference delay. The power on the sample was <10 mW for all measurements. The system reaches a measured sensitivity of −102 dB which is close to shot noise limit of ~103 dB when taking into account a 3 dB back coupling loss.

At a scan rate of 1.6 MHz, the time to acquire a 3D data set with 1000 x 1000 depth scans is theoretically 625 ms. However, such high speeds impose high demands on the 2D scanners

#172420 - $15.00 USD Received 13 Jul 2012; rev. 14 Sep 2012; accepted 15 Sep 2012; published 24 Sep 2012
(C) 2012 OSA

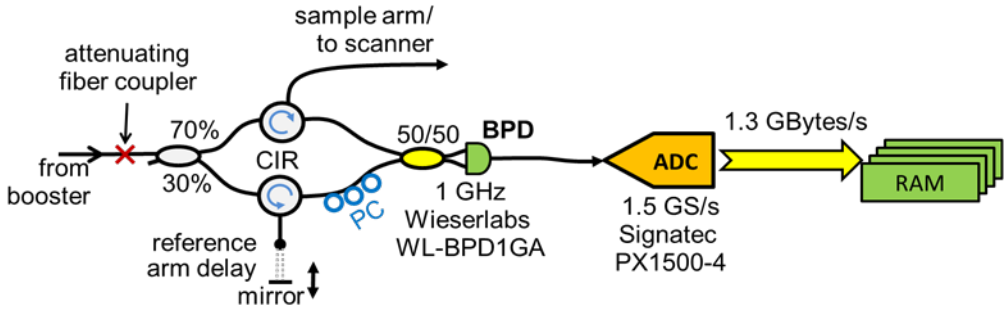


Fig. 2. Schematic of the interferometer and the data acquisition. Data is sampled at 1.5 GS/s and streamed into computer RAM. The data set size is only limited by available RAM. Bidirectional scanning allows an 85% scan duty cycle resulting in an average data transfer rate of ~1.3 GBytes/s.

used to raster the sample. To capture the volumetric data quickly, the fast scan axis was driven with a sinusoidal waveform of 680 Hz and bidirectional scanning was applied resulting in 2 complete B-frames per scanner cycle. Taking the most linear part of both scan directions, a total acquisition duty cycle of typically 85% is achieved. A dedicated post-processing step flips every second frame and also corrects for the non-linearity introduced by the sinusoidal scan [24]. The resulting 3D data set is free of interlacing artifacts.

The interferometer makes use of a 1 GHz dual balanced photoreceiver (Wieserlabs WL BPD1GA) and a 1.5 GS/s data acquisition card with a resolution of 8 bit (Signatec PX1500-4). As already reported previously [24,47], we find that 8 bit resolution is sufficient for good quality OCT provided that the available ADC range is well used. With the aid of specially coded software, the acquisition card is able to stream the sample data via PCIe directly into computer RAM so that the data set size is no longer limited by the amount of memory installed on the acquisition card itself. Due to the 85% scan duty cycle, the average sustained data rate is ~1.3 GBytes/s.

2.3. Scanning speed considerations

In order to acquire a full 3D volume without distortion caused by involuntary eye movements (saccades), the total 3D acquisition time should be kept below ~1 second [34,48] to avoid microsaccades. Higher acquisition times dramatically increase the probability of distortions introduced by saccades. At a 1.6 MHz depth scan rate and a 85% acquisition duty cycle, a 3D volume consisting of 1000 x 1000 depth scans can be conveniently acquired in 0.8 seconds. When scanning a field of 15 x 15 mm, this results in a scan speed on the sample of >20 m/s for the fast axis and ~19 mm/s for the slow axis. For a standard eye length of ~25 mm, the slow axis scan speed corresponds to an angular movement of ~90°/second which is faster than most saccades [49]. This means that for eye movements slower than that, a distorted but gap-free coverage of the sample can still be achieved. Due to gap-free coverage, the distortions can be corrected in post-processing.

3. Results

3.1. Power, sweep range and necessary detection bandwidth

The data acquisition speed is the critical bottleneck in this high speed OCT system: assuming a 85% scanning duty cycle, the applied digitizer can stream up to 1.5 GS/s during data acquisition. According to Nyquist's theorem, this translates into a usable fringe frequency limit of 750 MHz. The corresponding imaging range is 3.8 mm at a sweep range of 100 nm, as required for a resolution of 10 µm in tissue. While this is sufficient for the cornea or the chamber angle alone, the full anterior segment requires a larger imaging range. We apply the

#172420 - $15.00 USD Received 13 Jul 2012; rev. 14 Sep 2012; accepted 15 Sep 2012; published 24 Sep 2012
(C) 2012 OSA

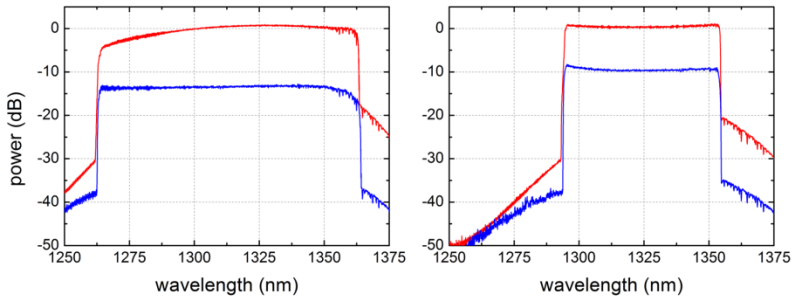


Fig. 3. Integrated spectra acquired with an optical spectrum analyzer for a 100 nm sweep range (left) as well as a 60 nm sweep range (right). The lower blue curve represents the FDML laser output while the red curve was measured after the buffer stage and the booster SOA.

concept of adjustable imaging range in FDML as described in [50], and sacrifice resolution to gain imaging range. We reduce the sweep range to 60 nm, hence, the Nyquist fringe frequency is shifted out to >6 mm and the resolution in tissue is degrades to 17 µm.

Accordingly, our system was operated and characterized in two operation modes: 100 nm sweep range ("high resolution mode") and 60 nm sweep range ("long range mode"). The sweep range of the FDML laser itself is limited primarily by the ~110 nm spectral width of the DCM in the cavity. However, since the booster SOA after the buffer stage amplifies much better on the red side than on the blue side, the best strategy is to move the sweep range slightly towards the red end, especially in the 60 nm mode. Figure 3 shows integrated spectra directly from the laser (blue curves) as well as after the booster SOA in the buffer stage (red curves). At 100 nm (60 nm), the laser output delivers 7 mW (10 mW) average power at a 25% duty cycle translating into 28 mW (40 mW) average power during on-time. The buffer stage and the booster SOA deliver a ~10 dB amplification (also shown in Fig. 3) resulting in an average power of 80 mW (100 mW) available for OCT imaging. For the anterior segment, this was attenuated to <10 mW on the sample for laser safety. The laser was operated with a center wavelength of 1312 nm (1324 nm).

3.2. Roll-off performance at 100 nm sweep range

Figure 4 shows two roll-off measurements performed with the same 1 GHz detector as in Fig. 2 but sampled with a 1 GHz oscilloscope (Tektronix DPO7104) at a real-time sampling rate of 10 GS/s. At 100 nm sweep range, the −6 dB roll-off point was measured at ~4.9 mm which corresponds to a fringe frequency of ~950 MHz. Due to detection bandwidth limitations, the true depth of the −6 dB point might actually be higher. The 2.6 MHz (1 MHz) OCT setup previously reported in [24] had a roll-off of 0.21 mm/dB (0.34 mm/dB) and a −6 dB imaging

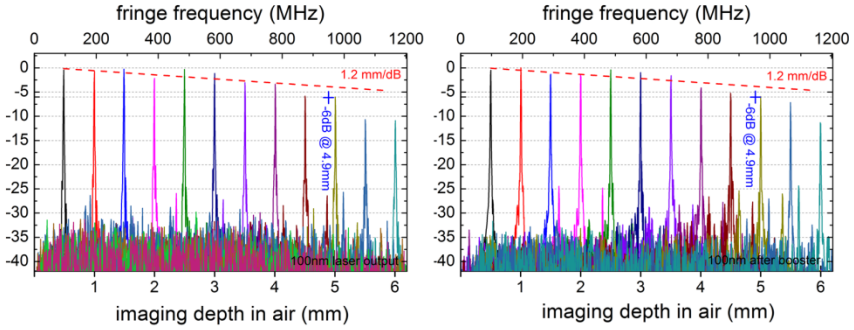


Fig. 4. Roll-off performance of the laser at 1.6 MHz for a sweep range over 100 nm. The left graph was measured directly at the laser output, the right graph after the buffer stage. The analog detection bandwidth was 1 GHz so part of the roll-off can be attributed to insufficient bandwidth. No apodizing was performed.

#172420 - $15.00 USD Received 13 Jul 2012; rev. 14 Sep 2012; accepted 15 Sep 2012; published 24 Sep 2012
(C) 2012 OSA

depth of 1.3 mm (2.0 mm). Hence, the new results presented here represent a ~4-fold improvement in roll-off performance.

As shown in Fig. 4, we find no roll-off degradation caused by the booster SOA in the buffer stage. Figure 5 shows a fringe interferogram acquired with a Mach-Zehnder interferometer with an arm length difference set to 10 mm corresponding to a 5 mm imaging depth (in air) and a fringe frequency of ~970 MHz. The analyzed light was coupled out behind the booster SOA. The figure shows the primary sweep (leftmost one) and the successive 3 buffered sweeps. The lower 3 graphs show zoomed-in sections of the fringes at 3 positions in the last sweep as indicated. As can be seen, the coherence and the fringe quality are not constant over the sweep but are found to degrade on the far red end. These phase jumps in the interferogram result in broadened point spread functions. During imaging, this effect is suppressed by use of a Hann or Kaiser window.

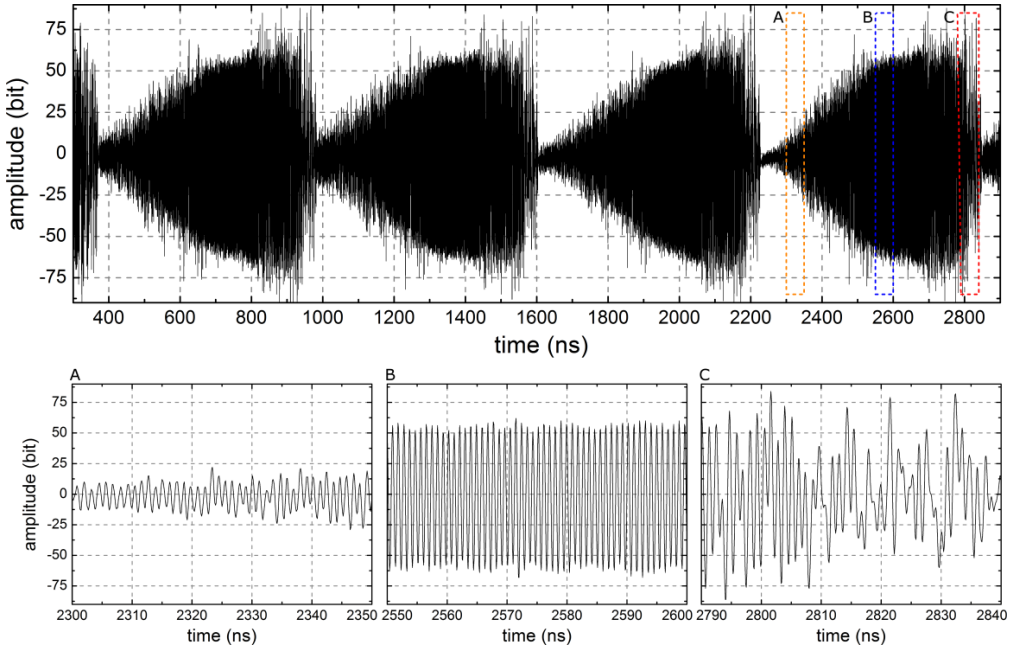


Fig. 5. Fringes at 1.6 MHz sweep rate over a 100 nm tuning range acquired with a Mach-Zehnder interferometer. The arm length difference was set to 10 mm corresponding to an imaging depth of 5 mm and a fringe frequency of ~970 MHz. The detection bandwidth was 1 GHz, the sampling rate 10 GS/s. The upper graph shows the interferogram acquired of 4 buffered sweeps while the lower graphs show zoomed-in sections marked A, B, C (left to right: orange, blue, red) in the upper graph.

3.3. Roll-off performance at 60 nm sweep range

In the "long range mode," the reduced sweep range translates into lower fringe frequencies at the same imaging depth. Figure 6 shows roll-off measurements at the laser output (left) and after the booster SOA (right) and can be directly compared to Fig. 4 (high resolution mode). Again, the −6 dB roll-off point is found to be at ~950 MHz close to the detection bandwidth. In contrast to the results at 100 nm sweep range, we measure a slight roll-off degradation caused by the booster SOA: the −6 dB imaging depth was measured at 8.4 mm for the laser output and at 8.2 mm behind the booster.

Furthermore, Fig. 6 shows "ghost peaks" ~10 dB below the major peaks. These peaks are caused within the FDML laser by a parasitic 17 mm cavity with weak reflection. This limits the usable imaging range to 8.5 mm which is beyond the usable imaging range due to the limited sampling rate of the digitizer applied for imaging.

#172420 - $15.00 USD Received 13 Jul 2012; rev. 14 Sep 2012; accepted 15 Sep 2012; published 24 Sep 2012
(C) 2012 OSA

3.4. Anterior segment imaging

Due to the rather steep roll-off of previous MHz-OCT systems, imaging was limited to highly scattering tissues such as skin. The good roll-off performance of the dispersion compensated FDML laser allows, for the first time, to perform high quality MHz-OCT imaging of deep and weakly scattering samples such as the human anterior segment.

Since the 1.5 GS/s ADC in the data acquisition only provides a usable image range up to its Nyquist frequency of 750 MHz, the two sweep ranges, 100 nm and 60 nm, are used for different purposes: the 100 nm sweep range provides a resolution of ~10 µm in tissue and allows imaging details spanning a depth of up to ~3.7 mm (in air). It is therefore useful for OCT of the chamber angle and the cornea (see Fig. 7). In contrast, the 60 nm sweep provides a reduced resolution of ~17 µm in tissue but on the other hand allows to image beyond 6 mm

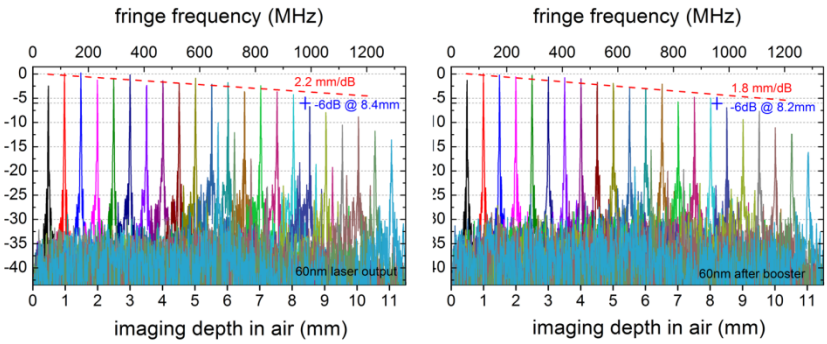


Fig. 6. Roll-off performance of the laser at 1.6 MHz for a sweep range over 60 nm. The left graph was measured directly at the laser output, the right graph after the buffer stage. The reduced sweep range compared to Fig. 4 reduces the resolution in tissue from 10 µm to 17 µm but moves the −6 dB roll-off point out from ~4.9 mm to >8 mm. Also, the 750 MHz Nyquist frequency of the 1.5 GS/s data acquisition card is moved from ~3.8 mm to >6 mm suitable for human anterior segment imaging. The dashed red line shows the approximate sensitivity roll-off taking into account depths up to Nyquist frequency.

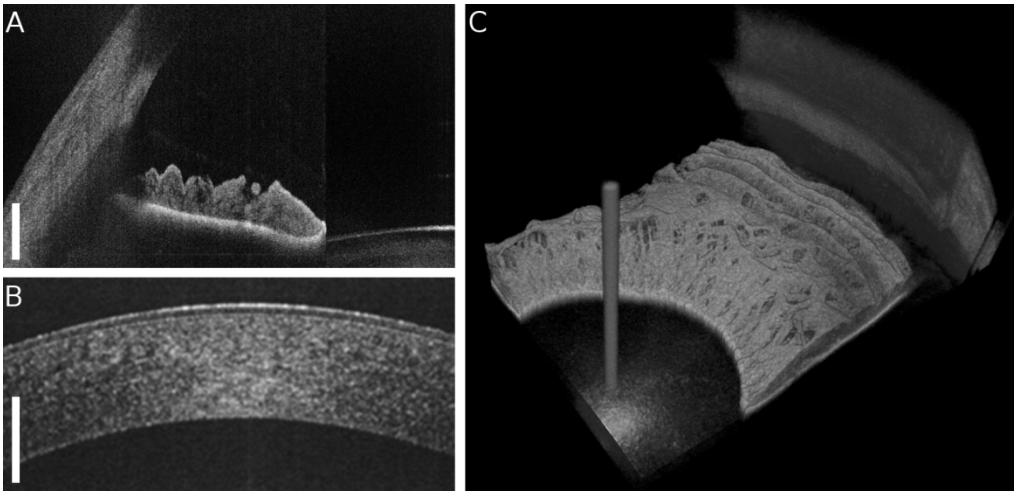


Fig. 7. (Media 1) OCT imaging at 100 nm sweep range and 1.6 MHz scan rate. (A) Chamber angle (885 A-scans, average over 4 frames). (B) Detail of the cornea near the center (430 depth scans, average over 10 frames). (C) 3D OCT data set of the anterior segment consisting of 1000 x 900 x 560 voxels (frames x depth scans x samples/scan) acquired in a total time of 0.8 seconds including galvanometer scanner dead times. Scale bars denote 0.5 mm in water.

#172420 - $15.00 USD Received 13 Jul 2012; rev. 14 Sep 2012; accepted 15 Sep 2012; published 24 Sep 2012
(C) 2012 OSA

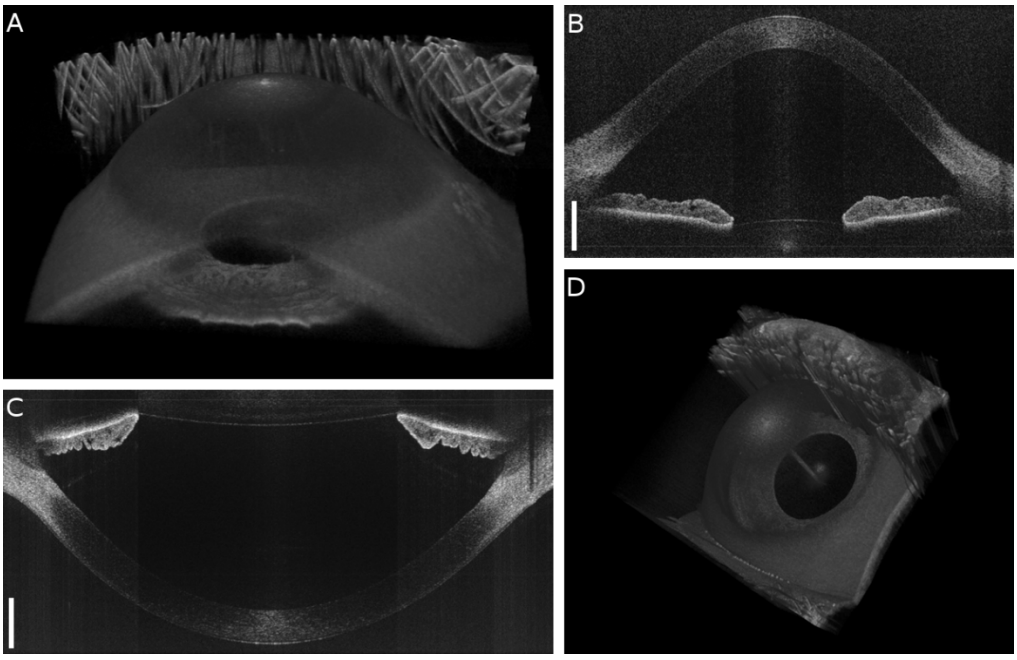


Fig. 8. OCT imaging at 60nm sweep range and 1.6 MHz scan rate. (A) 3D reconstruction of the whole anterior segment consisting of 1000 x 985 x 560 voxels (frames x depth scans x samples/scan) acquired in a total time of 0.8 seconds including galvanometer scanner dead times. (B) Single B-frame from extracted from the 3D data set on the left. (C) Anterior segment of dark-adapted human eye (average over 8 frames, 925 A-scans wide). (D) 3D reconstruction of a data set consisting of 1000 x 950 x 560 voxels, acquired in 0.8 seconds. Scale bars denote 1 mm in water.

depth which is sufficient for the whole anterior segment (see Fig. 8). All OCT data sets are shown as acquired, without any motion correction applied.

The image data using the high resolution mode (Fig. 7) exhibits good overall quality. We observe some increased noise levels along those A-scans with high scattering from the iris. The 2D representation of the chamber angle shows good image contrast, very few artifacts and even some signal from the region shadowed by the sclera. In the 2D image of the central cornea the layered internal structure is clearly visible, no side lobe artifacts at the air-tissue interface are visible and a clearly defined surface can be identified. The 3D representation in Fig. 7 (right) now shows the full potential of MHz imaging of the anterior segment. The entire data set is rich in detail over the whole depth range, increased noise caused by the highly scattering iris is almost not visible and no distortion due to motion artifacts can be identified. No motion correction algorithm and no eye tracking have been used. The potential of this undistorted MHz OCT data set for real volumetric topography mapping is obvious. The high isotropic sampling density of the A-scans aids the lively visualization of the fine and complex structure of the iris.

The images in Fig. 8, acquired in long range mode, still exhibit remarkable quality, despite the reduced axial resolution. Again the whole 3D data set is free of motion artifacts, because of the short acquisition time of 0.8 s. Due to the high sensitivity of the system of 102 dB, the single image of the whole cornea (Fig. 8 top, right) has acceptable quality even though no averaging has been applied.

6. Conclusion and outlook

We demonstrated, for the first time, an OCT setup which combines a good roll-off performance and a high speed of 1.6 MHz. This is a 16-fold improvement compared to our

#172420 - $15.00 USD Received 13 Jul 2012; rev. 14 Sep 2012; accepted 15 Sep 2012; published 24 Sep 2012
(C) 2012 OSA

previously published extended coherence FDML laser. The new dispersion compensated MHz-FDML laser at 1310 nm provides a roll-off performance which is suitable for imaging the whole anterior segment of the human eye. This allowed us to demonstrate the first MHz-OCT of the anterior segment. Densely sampled 3D data sets with ~1000 x 1000 A-scans were acquired within less than 1 second at a 85% acquisition duty cycle provided by bidirectional sinusoidal scanning.

FDML laser coherence and roll-off performance were improved by dispersion compensation in the FDML laser cavity. This allowed building a 4x buffered FDML laser with a sweep rate of 1.6 MHz and a −6 dB roll-off imaging depth beyond 4.9 mm. Due to the high speed and good coherence, the −6 dB roll-off point corresponds to fringe frequencies above 1 GHz and requires sampling rates in the GS/s range.

Several new clinically relevant applications of the system demonstrated here may be envisioned: a better visualization of defects and pathologies might be achieved by the higher definition 2D and 3D image data. More accurate shape measurements of the anterior segment might be possible due to reduced errors caused by motion artifacts. This would enable a more precise measurement of refractive power and higher order aberrations of the eye. Imaging extended microscopic structures with a high sampling density over a large area, e.g. imaging the trabecular meshwork, will also benefit from higher imaging speed. Considering the application in a clinical environment, the higher imaging speed might increase patient flow and thus reduce cost and improve patient comfort.

Acknowledgments

We would like to acknowledge the support from Prof. W. Zinth at the Ludwig-Maximilians-University Munich. This research was sponsored by the Emmy Noether program of the German Research Foundation (DFG – HU 1006/2-1), the European Union project FUN-OCT (FP7 HEALTH, contract no. 201880) and FDML-Raman (FP7 ERC, contract no. 259158).

#172420 - $15.00 USD Received 13 Jul 2012; rev. 14 Sep 2012; accepted 15 Sep 2012; published 24 Sep 2012
(C) 2012 OSA